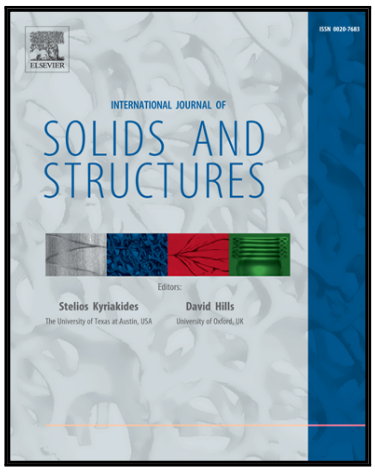

Topology optimization of periodic microstructures for enhanced loss factor using acoustic-structure interaction

Junghwan Kook , Jakob S. Jensen

PII: S0020-7683(17)30257-3
DOI: 10.1016/j.ijsolstr.2017.06.001
Reference: SAS 9605

To appear in: *International Journal of Solids and Structures*

Received date: 28 August 2016
Revised date: 24 April 2017
Accepted date: 1 June 2017

Please cite this article as: Junghwan Kook , Jakob S. Jensen , Topology optimization of periodic microstructures for enhanced loss factor using acoustic-structure interaction, *International Journal of Solids and Structures* (2017), doi: 10.1016/j.ijsolstr.2017.06.001

International Journal of Solids and Structures Revised manuscript

Topology optimization of periodic microstructures for enhanced loss factor using acoustic-structure interaction

Junghwan Kook* and Jakob S. Jensen

Centre for Acoustic-Mechanical Micro Systems (CAMM), Department of Electrical Engineering Technical University of Denmark, 2800 Kgs. Lyngby, Denmark

Submitted to **International Journal of Solids and Structures**

August 28, 2016

Revised April 24, 2017

Includes 8 figures and 1table

* Corresponding author Postal Address: Department of Electrical Engineering, Ørsteds Plads, Building 352, 2800 Kgs. Lyngby, Denmark

E-mail Address: junko@elektro.dtu.dk

Tel. +45 42478668

Abstract

In this work we present a topology optimization method for the design of 2D composite materials with a distribution of a solid constituent and a lossy acoustic medium for obtaining high loss factors. The method is based on a mixed displacement-pressure finite element (FE) formulation combined with the Bloch-wave condition. We solve the resulting FE eigenvalue problem on a repetitive unit cell with periodic boundary conditions and use a complex $\mathbf{k}(\omega)$ eigenvalue formulation to compute the loss factor. We consider the optimization problem of maximizing the loss factor in a target frequency range with an additional constraint on the stiffness. In the provided example we demonstrate the effect of combined local resonators and acoustic resonances of similar frequency for creating an enhanced overall loss factor of the material.

Keywords; Topology optimization, Acoustic-Structure Interaction (ASI), loss factor, microstructure

1. Introduction

In many structural applications it is desirable to use materials that have high stiffness and also the ability to damp mechanical vibrations. Promising candidates are microstructured composite materials that may display a favorable combination of these properties that cannot be found to a similar extent in a single material constituent.

However, it is an obvious design challenge to create a composite microstructure that yields high damping without sacrificing stiffness. In this respect topology optimization is a valuable design tool. The topology optimization method is based on free distribution of material constituents in a designated design domain with the aim of obtaining the best possible performance within a set of specified constraints. Potentially, this allows engineers to conceive efficient conceptual designs that fulfill essential requirements in the early design phase. The method has successfully been applied to numerous engineering fields such as structural mechanics, mechanisms, fluids, and electromagnetics (Bendsoe and Sigmund, 2004). Topology optimization has also been applied to design composite materials with unique properties such as negative Poisson's ratio (Andreassen et al., 2014), negative thermal expansion coefficients (Sigmund and Torquato, 1997) and bandgap structures (Halkjær et al., 2006; Bilal and Hussein, 2011).

Topology optimization techniques for designing composite microstructures with a lossy compliant and a stiff constituent have emerged in recent years (Meaud et al., 2013; Andreasen et al., 2014). Typical optimization objectives considered have been extreme storage and loss moduli of the viscoelastic composites. In the quasi-static region the loss factor is effectively limited by the loss factor of the involved materials, but for higher frequencies the loss (or attenuation) factor can be enhanced considerably by resonances and wave interference effects (Andreassen and Jensen, 2013b). The present study is closely related to the work in (Andreassen and Jensen,

2013b) but here we consider the effect of replacing the lossy/soft material constituent with an acoustic medium and hence, rather than solving a pure structural dynamic problem, we need to consider the acoustic-structure interaction effects involved. To the best of our knowledge, this is the first work that develops the topology optimization framework for periodic microstructures involving acoustic-structure interaction (ASI).

The topology optimization procedure in this work is adapted from (Andreassen and Jensen, 2013a, b) in which the so-called $\mathbf{k}(\omega)$-formulation is used for computing the dynamic properties of the viscoelastic composite material. However, it is here applied in combination with a mixed finite element formulation in order to model the acoustic-structure interaction. The mixed finite element formulation was earlier introduced for enabling topology optimization of acoustic-structure interaction problems (Sigmund and Clausen, 2007; Yoon et al., 2007). The main challenge is here to develop a formulation that allows structural domains to change into acoustic domains and vice versa – a scenario which is difficult to achieve with density-based topology optimization schemes based on standard finite element methods. An alternative way to elegantly circumvent the problem associated with the two physical domains, is the level set method that allows for a natural division of the structural and acoustic domains (Shu et al., 2014). Pros and cons of level set methods vs. density-based topology optimization methods have been thoroughly discussed in (Sigmund and Maute, 2013) and can be expected to apply directly for the application to acoustic-structure interaction problems as well. Recently, other works have appeared on topology optimization of acoustic-structure interaction problems, however, without the possibility for modifying the interface between acoustic and structural domains (Picelli et al., 2015; Søndergaard and Pedersen, 2014; Vicente et al., 2015)

With an acoustic medium, e.g. air, instead of a viscoelastic material it becomes significantly more challenging to obtain high losses since the acoustic medium possesses a comparatively low intrinsic loss. However, in a recent study (Kook and Jensen, 2014) we demonstrated the possibility for enhancement of the damping ratio of a structure with microbeam resonators embe dded in internal air cavities, results also supported by experimental observations. In the present paper we aim to exploit and enhance such effects in a topology optimization framework. Also it should be mentioned that an additional benefit of replacing the soft material constituent by air is

manufacturability. Usually, the stiff constituent is printed and then infused with the soft constituent. Thus, the printed microstructure acts as a mold for the soft material. However, the manufacturability of such a combination, perhaps involving a complicated geometry, is always a challenge. When designing the elasto-acoustic composite, using air rather than a soft constituent can help overcome such difficulties.

The paper is organized as follows. In Section 2, we describe the mixed displacement-pressure finite element formulation combined with the Bloch-wave condition applied to the governing equations. The eigenvalue problems with $\mathbf{k}(\omega)$ and $\omega(\mathbf{k})$ -formulations are introduced. In section 3, the topology optimization problem is stated with the loss factor computed by eigensolutions of the developed $\mathbf{k}(\omega)$ -formulation. Design variables and material interpolation functions are introduced for topology optimization of acoustic–structure interaction problems using the mixed displacement-pressure finite element formulation and the design sensitivity analysis needed for the optimization algorithm is described in detail. In Section 4, the resulting microstructure optimized for maximum loss is presented and we discuss the effects of the presence of an acoustic medium and viscous properties. Finally, conclusions are given in Section 5.

2. Physical model

2.1 Mixed $\mathbf{u}/p$ formulation

Acoustic-structure interaction (ASI) involves the coupling between an acoustic pressure field and the structural displacement field. In the general procedure these fields are treated separately and the mutual acoustic-structure coupling is obtained by imposing explicit boundary conditions. At the boundary the acoustic pressure acts as a load on the structural domain, and the structural acceleration in turn affects the acoustic domain in the form of a normal acceleration across the acoustic-structure boundary. However, this segregated approach is not directly applicable to a topology optimization procedure since the final boundaries is an end product of the optimization procedure and not known a priori. As an alternative, the use of a mixed finite element formulation with both displacements ($\mathbf{u}$) and pressure (p) as primary variables (a $\mathbf{u}/p$ formulation) in connection with topology optimization has been proposed (Sigmund and

Clausen, 2007; Yoon et al., 2007). In order to facilitate modeling and optimization of elasto-acoustic composites, we employ the mixed **u**/*p* formulation here as well. In this way the explicit formulation of the boundary between the material constituents is circumvented, which facilitates the use of an iterative material distribution algorithm.

As a starting point we consider in-plane wave propagation in a linear elastic medium

$$\sigma_{ij,j} = \rho \frac{\partial^2 u_i}{\partial t^2} \tag{1}$$

where σ_{ij} is the symmetric stress tensor, ρ the material density and u_i the displacement components. We use the constitutive relation in terms of bulk modulus K and shear modulus G

$$\sigma_{ij} = K\varepsilon_V \delta_{ij} + 2G\varepsilon'_{ij} \tag{2}$$

where the strain is split into the volumetric strain tensor $\varepsilon_V = \Delta V/V = \varepsilon_{kk}$ and the deviatoric strain $\varepsilon'_{ij} = \varepsilon_{ij} - \frac{1}{2}\varepsilon_V \delta_{ij}$. For 2D-plane strain the value of the shear and bulk moduli in terms of Young's modulus E and Poisson's ratio ν are defined as follows:

$$K = \frac{E}{2(1+\nu)(1-2\nu)}, \quad G = \frac{E}{2(1+\nu)} \tag{3}$$

We also introduce the pressure as an auxiliary variable in the form of the pressure and volumetric strain relationship:

$$p = -K\varepsilon_V \tag{4}$$

After inserting each strain tensor expression into Eq. (2), the equilibrium conditions for the mixed formulation can be written in strong form as:

$$\boldsymbol{\partial}^{\mathrm{T}}\left(\mathbf{G}\boldsymbol{\partial}\mathbf{u}-\mathbf{p}\right)=\rho\ddot{\mathbf{u}}$$

$$\boldsymbol{\partial}=\begin{bmatrix}\dfrac{\partial}{\partial x} & 0\\ 0 & \dfrac{\partial}{\partial y}\\ \dfrac{\partial}{\partial y} & \dfrac{\partial}{\partial x}\end{bmatrix},\qquad \mathbf{G}=\begin{bmatrix}G & -G & 0\\ -G & G & 0\\ 0 & 0 & G\end{bmatrix} \tag{5}$$

$$\nabla\cdot\mathbf{u}+\frac{p}{K}=0 \tag{6}$$

It has been demonstrated that by varying the shear modulus G and the bulk modulus K between representative values for an acoustic and structural domain, respectively, we can use this monolithic formulation to describe the problem of acoustic-structure interaction. Thus, for topology optimization, we can freely assign air and solid medium to the design domain and do not need an explicit formulation of the boundary between the domains. For further details of the mixed $\mathbf{u}/p$ formulation in connection with topology optimization for acoustic-structure interaction see (Yoon et al., 2007). In present paper, the mixed $\mathbf{u}/p$ formulation combined with the Bloch-wave condition is applied to the governing equations. To our knowledge, this is the first work to consider the full dynamic model of the mixed $\mathbf{u}/p$ formulation and its extension to topology optimization for elasto-acoustic composites.

2.2 Wave propagation in periodic medium

In the case of a periodic medium the wave solution to the full dynamic problem can be reduced by employing the Bloch-wave theorem (Bloch, 1929). In the mixed formulation, we have two waves for displacement and pressure fields, respectively. Thus we assume solutions of the form

$$\mathbf{u}(\mathbf{x},t)=\tilde{\mathbf{u}}(\mathbf{x})e^{i\mathbf{k}^{\mathrm{T}}\mathbf{x}}e^{i\omega t} \tag{7}$$

$$\mathbf{p}(\mathbf{x},t)=\tilde{\mathbf{p}}(\mathbf{x})e^{i\mathbf{k}^{\mathrm{T}}\mathbf{x}}e^{i\omega t} \tag{8}$$

where ω is the wave frequency, $\mathbf{k}=(k_x,k_y)^{\mathrm{T}}$ is a plane wave vector, $e^{i\omega t}$ represents the time-

harmonic dependency of the solution, and $\tilde{\mathbf{u}}$ and $\tilde{\mathbf{p}}$ are periodic displacement and pressure fields, respectively. This means that we split the solution into three parts: one (periodic) in the local unit cell, one giving the spatial periodicity, and a final one giving the temporal periodicity. The Bloch-wave theorem allows us to solve the eigenvalue problem for a single unit cell only. The wave vector $\mathbf{k}$ must be varied within the irreducible Brillouin zone, which is illustrated in Fig. 1(b) for a two-dimensional periodic structure consisting of a solid phase and air.

We insert the Bloch-wave expansions into the mixed $\mathbf{u}/p$ formulation before discretizing the problem. Inserting Eqs. (7) and (8) into Eq. (5) yields the following equation

$$\partial^{\mathrm{T}}\left(\mathbf{G}\left(\partial\tilde{\mathbf{u}}+\partial(i\mathbf{k}^{\mathrm{T}}\mathbf{x})\tilde{\mathbf{u}}\right)e^{i\mathbf{k}^{\mathrm{T}}\mathbf{x}}\right)-\left(\partial^{\mathrm{T}}\tilde{\mathbf{p}}+\partial^{\mathrm{T}}(i\mathbf{k}^{\mathrm{T}}\mathbf{x})\tilde{\mathbf{p}}\right)e^{i\mathbf{k}^{\mathrm{T}}\mathbf{x}}=-\rho\omega^{2}\tilde{\mathbf{u}}e^{i\mathbf{k}^{\mathrm{T}}\mathbf{x}} \tag{9}$$

in which the exponential time-dependent term has been divided out. This can be rewritten as

$$\partial^{\mathrm{T}}\left(\mathbf{G}\left(\partial\tilde{\mathbf{u}}+i\left(\boldsymbol{\alpha}_1 k_x+\boldsymbol{\alpha}_2 k_y\right)\tilde{\mathbf{u}}\right)e^{i\mathbf{k}^{\mathrm{T}}\mathbf{x}}\right)-\left(\partial^{\mathrm{T}}\tilde{\mathbf{p}}+i\left(\boldsymbol{\alpha}_1^{\mathrm{T}} k_x+\boldsymbol{\alpha}_2^{\mathrm{T}} k_y\right)\tilde{\mathbf{p}}\right)e^{i\mathbf{k}^{\mathrm{T}}\mathbf{x}}=-\rho\omega^{2}\tilde{\mathbf{u}}e^{i\mathbf{k}^{\mathrm{T}}\mathbf{x}} \tag{10}$$

where, k_x and k_y are wave vector components in the x and y-direction, respectively, and

$$\boldsymbol{\alpha}_1=\begin{bmatrix}1 & 0\\ 0 & 0\\ 0 & 1\end{bmatrix},\quad \boldsymbol{\alpha}_2=\begin{bmatrix}0 & 0\\ 0 & 1\\ 1 & 0\end{bmatrix} \tag{11}$$

The differential operator in Eq. (5) can thus be written as

$$\partial^{\mathrm{T}}=\boldsymbol{\alpha}_1^{\mathrm{T}}\frac{\partial}{\partial x}+\boldsymbol{\alpha}_2^{\mathrm{T}}\frac{\partial}{\partial y} \tag{12}$$

and by introducing the definition

$$\boldsymbol{\kappa}=i\left(\boldsymbol{\alpha}_1 k_x+\boldsymbol{\alpha}_2 k_y\right) \tag{13}$$

then we can write Eq. (10) as

$$\boldsymbol{\alpha}_1^{\mathrm{T}}\frac{\partial}{\partial x}\left(\mathbf{G}\left(\partial\tilde{\mathbf{u}}+\boldsymbol{\kappa}\tilde{\mathbf{u}}\right)e^{i\mathbf{k}^{\mathrm{T}}\mathbf{x}}\right)+\boldsymbol{\alpha}_2^{\mathrm{T}}\frac{\partial}{\partial y}\left(\mathbf{G}\left(\partial\tilde{\mathbf{u}}+\boldsymbol{\kappa}\tilde{\mathbf{u}}\right)e^{i\mathbf{k}^{\mathrm{T}}\mathbf{x}}\right)-\left(\partial^{\mathrm{T}}\tilde{\mathbf{p}}+\boldsymbol{\kappa}^{\mathrm{T}}\tilde{\mathbf{p}}\right)e^{i\mathbf{k}^{\mathrm{T}}\mathbf{x}}=-\rho\omega^{2}\tilde{\mathbf{u}}e^{i\mathbf{k}^{\mathrm{T}}\mathbf{x}} \tag{14}$$

and after further manipulations we obtain

$$\begin{aligned}&\boldsymbol{\alpha}_1^{\mathrm{T}}\left(\frac{\partial}{\partial x}\mathbf{G}\left(\boldsymbol{\partial}\tilde{\mathbf{u}}+\boldsymbol{\kappa}\tilde{\mathbf{u}}\right)\right)e^{i\mathbf{k}^{\mathrm{T}}\mathbf{x}}+\boldsymbol{\alpha}_1^{\mathrm{T}}\mathbf{G}\left(\boldsymbol{\partial}\tilde{\mathbf{u}}+\boldsymbol{\kappa}\tilde{\mathbf{u}}\right)\left(\frac{\partial e^{i\mathbf{k}^{\mathrm{T}}\mathbf{x}}}{\partial x}\right)+\boldsymbol{\alpha}_2^{\mathrm{T}}\left(\frac{\partial}{\partial y}\mathbf{G}\left(\boldsymbol{\partial}\tilde{\mathbf{u}}+\boldsymbol{\kappa}\tilde{\mathbf{u}}\right)\right)e^{i\mathbf{k}^{\mathrm{T}}\mathbf{x}}\\&+\boldsymbol{\alpha}_2^{\mathrm{T}}\mathbf{G}\left(\boldsymbol{\partial}\tilde{\mathbf{u}}+\boldsymbol{\kappa}\tilde{\mathbf{u}}\right)\left(\frac{\partial e^{i\mathbf{k}^{\mathrm{T}}\mathbf{x}}}{\partial y}\right)-\left(\boldsymbol{\partial}^{\mathrm{T}}\tilde{\mathbf{p}}+\boldsymbol{\kappa}^{\mathrm{T}}\tilde{\mathbf{p}}\right)e^{i\mathbf{k}^{\mathrm{T}}\mathbf{x}}=-\rho\omega^2\tilde{\mathbf{u}}e^{i\mathbf{k}^{\mathrm{T}}\mathbf{x}}\end{aligned}\tag{15}$$

Expanding the derivative of the exponential terms and dividing out the remaining exponential terms yields

$$\begin{aligned}&\boldsymbol{\alpha}_1^{\mathrm{T}}\left(\frac{\partial}{\partial x}\mathbf{G}\left(\boldsymbol{\partial}\tilde{\mathbf{u}}+\boldsymbol{\kappa}\tilde{\mathbf{u}}\right)\right)+\boldsymbol{\alpha}_2^{\mathrm{T}}\left(\frac{\partial}{\partial y}\mathbf{G}\left(\boldsymbol{\partial}\tilde{\mathbf{u}}+\boldsymbol{\kappa}\tilde{\mathbf{u}}\right)\right)+ik_x\boldsymbol{\alpha}_1^{\mathrm{T}}\mathbf{G}\left(\boldsymbol{\partial}\tilde{\mathbf{u}}+\boldsymbol{\kappa}\tilde{\mathbf{u}}\right)+ik_y\boldsymbol{\alpha}_2^{\mathrm{T}}\mathbf{G}\left(\boldsymbol{\partial}\tilde{\mathbf{u}}+\boldsymbol{\kappa}\tilde{\mathbf{u}}\right)\\&-\left(\boldsymbol{\partial}^{\mathrm{T}}\tilde{\mathbf{p}}+\boldsymbol{\kappa}^{\mathrm{T}}\tilde{\mathbf{p}}\right)=-\rho\omega^2\tilde{\mathbf{u}}\end{aligned}\tag{16}$$

and after gathering terms with Eqs. (12) and (13), Eq. (5) combined with the Bloch-wave expansion can be written as

$$\boldsymbol{\partial}^{\mathrm{T}}\left(\mathbf{G}\boldsymbol{\partial}\tilde{\mathbf{u}}\right)+\boldsymbol{\partial}^{\mathrm{T}}\left(\mathbf{G}\boldsymbol{\kappa}\tilde{\mathbf{u}}\right)+\boldsymbol{\kappa}^{\mathrm{T}}\mathbf{G}\left(\boldsymbol{\partial}\tilde{\mathbf{u}}+\boldsymbol{\kappa}\tilde{\mathbf{u}}\right)-\left(\boldsymbol{\partial}^{\mathrm{T}}\tilde{\mathbf{p}}+\boldsymbol{\kappa}^{\mathrm{T}}\tilde{\mathbf{p}}\right)=-\rho\omega^2\tilde{\mathbf{u}}\tag{17}$$

which should be supplemented by a standard periodic condition imposed on the unit cell boundary.

In a similar fashion we can obtain the pressure and volumetric strain relationship in Eq. (6) combined with the Bloch-wave expansion as

$$\nabla\cdot\tilde{\mathbf{u}}+\tilde{\boldsymbol{\kappa}}\tilde{\mathbf{u}}+\frac{1}{K}\tilde{p}=0\tag{18}$$

where we have defined

$$\begin{aligned}&\tilde{\boldsymbol{\kappa}}=i\boldsymbol{\beta}_1k_x+i\boldsymbol{\beta}_2k_y,\\&\boldsymbol{\beta}_1=\begin{bmatrix}1 & 0\end{bmatrix},\quad \boldsymbol{\beta}_2=\begin{bmatrix}0 & 1\end{bmatrix}\end{aligned}\tag{19}$$

We now convert the preceding equations to their weak form, suitable for the finite element method. The equilibrium condition for the formulation can be written as

$$\begin{aligned}&\int_\Omega\delta\tilde{\mathbf{u}}\cdot\left(\boldsymbol{\partial}^{\mathrm{T}}(\mathbf{G}\boldsymbol{\partial}\tilde{\mathbf{u}})\right)\mathrm{d}\Omega+\int_\Omega\delta\tilde{\mathbf{u}}\cdot\left(\boldsymbol{\partial}^{\mathrm{T}}(\mathbf{G}\boldsymbol{\kappa}\tilde{\mathbf{u}})\right)\mathrm{d}\Omega+\int_\Omega\delta\tilde{\mathbf{u}}\cdot\left(\boldsymbol{\kappa}^{\mathrm{T}}\mathbf{G}(\boldsymbol{\partial}\tilde{\mathbf{u}}+\boldsymbol{\kappa}\tilde{\mathbf{u}})\right)\mathrm{d}\Omega\\&-\int_\Omega\delta\tilde{\mathbf{u}}\cdot\left(\boldsymbol{\partial}^{\mathrm{T}}\tilde{\mathbf{p}}+\boldsymbol{\kappa}^{\mathrm{T}}\tilde{\mathbf{p}}\right)\mathrm{d}\Omega+\int_\Omega\delta\tilde{\mathbf{u}}\cdot\left(\omega^2\rho\tilde{\mathbf{u}}\right)\mathrm{d}\Omega=0\end{aligned}\tag{20}$$

and the weak form of Eq. (18) takes the following form:

$$\int_{\Omega} \delta\tilde{p}\left(\nabla\cdot\tilde{\mathbf{u}}+\tilde{\boldsymbol{\kappa}}\tilde{\mathbf{u}}+\frac{1}{K}\tilde{p}\right)\mathrm{d}\Omega=0 \tag{21}$$

Eqs. (20) and (21) must be satisfied for all kinematically admissible displacement variations $\delta\tilde{u}$ and pressure variations $\delta\tilde{p}$.

We now solve the eigenvalue problem along the irreducible Brillouin zone bounded by the line O-A-B-O in Fig. 1(b). Generally, solving for the frequency ω at a specified wave vector $\mathbf{k}$ ($\omega(\mathbf{k})$-formulation), yields a band diagram that illustrates the dispersion properties, with the frequencies plotted versus the wave vector along the boundary of the irreducible Brillouin zone.

Alternatively, one can specify the frequency and solve for the wave vector ($\mathbf{k}(\omega)$-formulation). In the presence of losses the two formulations result either in complex frequencies or complex wave vectors. In this work we choose the $\mathbf{k}(\omega)$-formulation which provides a direct measure of the spatial attenuation. Additionally, the $\mathbf{k}(\omega)$-formulation offers the advantage to handle frequency dependent material properties (which we do not apply in this work however). With the choice of the $\mathbf{k}(\omega)$-formulation, we reformulate the mixed $\mathbf{u}/p$ formulation combined with the Bloch-wave expansion as an eigenvalue problem in terms of the wave number. The wave vector components in Eqs. (20) and (21) are expressed in terms of a scalar wavenumber k and the direction of propagation as

$$k_x = k\cos(\theta),\ \ k_y = k\sin(\theta) \tag{22}$$

where θ is the angle determining the wave propagation direction as illustrated in Fig. 1(b). In this paper topology optimization is carried out for microstructures restricted to possess 45 degree symmetry. Thus we can limit our search in the irreducible Brillouin zone to the line O-A-B-O in Fig. 1(b). Thus, in order to cover a wavenumber range corresponding to the irreducible Brillouin zone the developed $\mathbf{k}(\omega)$-formulation should be solved by choosing different values θ in the range from 0 to 45 degree.

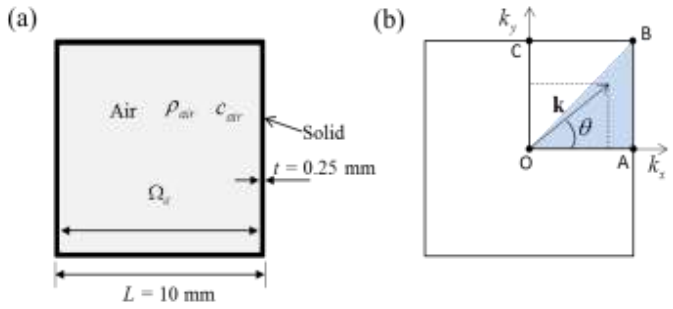

Figure 1 (a) Unit cell of periodic microstructure with an acoustic cavity surrounded by the structure of thickness, t=0.25 mm. The side length of the cell is L=10 mm. (b) Illustration of the Brillouin zone and propagation directions specified by the angle θ. For materials with 45° symmetry the irreducible Brillouin Zone for a unit cell is the domain bounded by the line O-A-B-O.

The solution to the eigenvalue problem using the $\mathbf{k}(\omega)$ -formulation is in the form of a complex wave number $k = k' + ik''$. The real part, k' represents the spatial periodicity and the imaginary part, k'' represents the spatial attenuation of the propagation. The attenuation factor can be computed form the ratio of the imaginary and complex parts as follows (Cremer et al., 2005)

$$\eta = 2\frac{k''}{k'} \tag{23}$$

It is noted that maximization of the minimum attenuation factor for a given frequency, ω and a wave propagation direction, θ is considered as an objective function for our subsequent optimization procedure.

Using the Galerkin method, the mixed **u**/p formulation specified with the wave vector components in Eq. (22) can be transformed to a discrete residual equation for the eigenvalue problem by specifying ω and solving for the complex wave number k. In this work we use COMSOL 4.4 Multiphysics for the implementation. The finite element discretization in COMSOL leads to the generalized eigenvalue problem:

$$\left[k^2\mathbf{M}(\theta) + k\mathbf{C}(\theta) + \mathbf{K}(\omega^2)\right]\mathbf{U} = 0 \tag{24}$$

where $\mathbf{U}$ is the solution vector, $\mathbf{M}$ is the mass matrix, $\mathbf{C}$ is the damping matrix, $\mathbf{K}$ is the

stiffness matrix. Instead of solving the quadratic eigenvalue problem directly we reformulate it into a linear eigenvalue problem using a standard approach (Moiseyenko and Laude, 2011).

2.3 Numerical test

First we present a validation of the $\mathbf{k}(\omega)$-formulation by comparing band diagrams obtained with the $\omega(\mathbf{k})$-formulation solved by a standard Acoustic-Structure Interaction (ASI) model and the $\mathbf{k}(\omega)$-formulation solved with the mixed **u**/*p* model. For further details of the investigation of the $\mathbf{k}(\omega)$-formulation see (Moiseyenko and Laude, 2011; Andreassen and Jensen, 2013a; Wang et al., 2015).

As a representative periodic microstructure we consider the unit cell with an encapsulated acoustic cavity as illustrated in Fig. 1(a). For the solid domain, a Young's modulus $E_0 = 2$ GPa, and the mass density $\rho = 1000$ kg/m^3 have been chosen. For structural damping we use a complex Young's modulus, so that $E_c = E_0(1+i\eta_{sol})$ and to model a lossy acoustic medium we apply a phenomenological model with a complex speed of sound $c_c = c_0(1+i\eta_{air})$ in which η_{air} is an acoustic loss factor. It should be noted that in (Kook and Jensen, 2014), the phenomenological model was demonstrated to provide qualitative similar results when compared to a more advanced thermoacoustic-structure interaction model, however, at a significantly reduced computational cost.

The material values used in the mixed **u**/p formulation seen in Eq. (3) are the complex bulk and shear modulus for the solid phase, K_s and G_s and the bulk modulus for air determined by $K_a = \rho_a c_c^2$ with the speed of sound $c_0 = 343$ m/s and the air density $\rho_a = 1.25$ kg/m^3 (the shear modulus in the acoustic domain is set to zero). In all examples in this paper we employ the structural loss, η_{sol} and the acoustical loss η_{air} as 1.0e-3 and 1.0e-2, respectively.

For the mixed **u**/*p* formulation, an appropriate finite element implementation must satisfy the inf-sup condition (Wang and Bathe, 1997). All numerical tests and the topology optimization

problem are discretized using 4-node quadrilateral elements with bi-linear displacement and piece-wise constant pressure, called Q-4/1. These elements are known to be only partially stable due to spurious modes in the eigensolution. Here, we discard spurious modes by selecting only modes with a larger real part than a chosen shift value. Using this strategy and employing the Q-4/1 element with maximum length of the element, ($h_{\max} = 0.125$ mm) we effectively obtain robust solutions necessary for employing our topology optimization method.

Fig. 2(a) illustrates the comparison between the two formulations and it is observed that the results agree perfectly. We also plot the smallest attenuation factor for all propagating angles θ, within the irreducible Brillouin zone as a function of the frequency as seen in Fig 2(b). A high attenuation factor is observed in the frequencies where the corresponding band diagram shows significant band distortion and flat bands (either acoustic modes or low group velocity). For other frequencies the loss factor is close to the value for the structural loss: 1.0e-3.

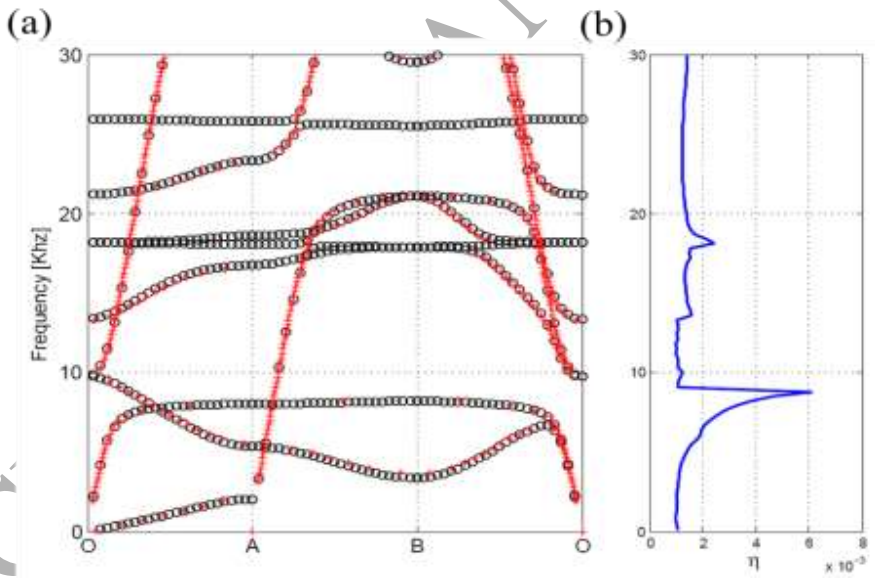

Figure 2 (a) Band diagrams for the microstructure consisting of acoustic and structure domain. The $\omega(\mathbf{k})$-formulation has been solved for 25 points along with the bounded line O-A-B-O for first eight eigenvalues (shown as circles). The $\mathbf{k}(\omega)$-formulation has been solved for a range of wave frequencies $\omega \in [0,30]$ khz (shown as crosses), (b) Illustration of the minimum attenuation factor among different propagating angle for given frequencies.

3. The topology optimization problem

3.1 Material interpolation

We solve the resulting FE eigenvalue problem on a repetitive unit cell with periodic boundary conditions and use a complex **k**(ω) eigenvalue formulation in order to compute the loss factor for given wave frequencies. Based on this modeling approach our goal is to find an optimized material distribution by using a gradient-based topology optimization formulation (Andreassen and Jensen, 2013b).

We introduce a continuous element design variable $0<\gamma_i<1$ to interpolate the element material properties between air and solid so that the mixed finite element governing equation can alternate between the Helmholtz equation and the linear elasticity equation. The proper choice of interpolation function deserves careful attention in the topology optimization problem to deliver discrete '0-1' optimal designs and to avoid spurious modes for the eigenvalue problem (Pedersen, 2014). Here, we apply a RAMP interpolation (Rational Approximation of Material Properties) based on the bulk and shear modulus and material density as in the following (Yoon et al., 2007):

$$K(\gamma)=K_a+\left(\frac{\gamma}{1+(1-\gamma)p_K}\right)(K_s-K_a) \tag{25}$$

$$G(\gamma)=G_s\left(\frac{\gamma}{1+(1-\gamma)p_G}\right) \tag{26}$$

$$\rho(\gamma)=\rho_s\gamma+\rho_a(1-\gamma) \tag{27}$$

The design variable γ governs the distribution of air and solid material in the design domain, so that when γ = 0, the element material property corresponds to air. On the contrary, a solid material is obtained when γ = 1. The two constants p_K and p_G are introduced in the interpolation functions for the element shear and bulk modulus as penalization parameters. These can be chosen in order to help eliminate intermediate design variables in the final design. For acoustic-structure interaction problems no rigorous guidelines exists for choosing the values of

these parameters but by using a trial-and-error approach we have found that a choice of $p_G = p_K = 4$ works well for the problems considered.

The optimization problem is to maximize the minimum loss factor in a prescribed frequency ranges for any direction of wave vector in order to obtain the largest possible wave decay. Thus, the formulation for the optimization problem takes form as:

$$\begin{aligned} \max_{\gamma} \ &: \ \min_{\theta} \left\{ \tilde{\eta}_\theta = \sum_i \eta(\omega_i) \right\} \\ &: \left[k^2 \mathbf{M}(\theta) + k\mathbf{C}(\theta) + \mathbf{K}(\omega^2) \right] \mathbf{U} = 0 \\ &: 0 < \gamma_i < 1 \end{aligned} \tag{28}$$

where the function evaluation $\tilde{\eta}_\theta$ is the summation of all loss factors computed for a target frequency range. The max-min optimization problem is solved using the bound formulation as an alternative to Eq. (28). For this purpose we introduce an artificial optimization variable z and restate the original optimization problem as;

$$\begin{aligned} &\max_{\gamma} \ : z \\ &\text{subject to} : \tilde{\eta}_\theta \geq z \quad \theta \in \left[0^\circ, \ 22.5^\circ, \ 45^\circ \right] \end{aligned} \tag{29}$$

where the new artificial variable z is introduced. We have found that considering the three angles in the formulation is sufficient to obtain stable optimization results (the validity of the results has then been checked using more angles).

In order to define a well-posed optimization and to obtain applicable 0-1 designs, the optimization problems can be modified with several regularization schemes. In order to avoid designs with small structural features, which make the design inconvenient to fabricate, the threshold projection method (Wang et al., 2010) is employed with a constant filter radius, R, that describes the desired minimum length scale of features.

The mixed **u**/p formulation may generate designs which contain solid (porous) islands surrounded by air. This is, from a fabrication point of view, unsatisfactory since the islands are not connected to the unit cell. In order to circumvent this problem we introduce an additional

constraint on the optimization problem. The homogenized elasticity modulus E^H of the composite is computed by numerical homogenization of the corresponding static structural problem (without acoustic domain) and required to be larger than a specified threshold. Thus the stiffness constraint is formulated as;

$$E^H \geq f_E E_0 \tag{30}$$

where f_E is a positive real constant that specifies the desired fraction of the elastic modulus of the solid material. Further details of the computation of E^H and corresponding sensitivities can be found in several papers e.g. (Sigmund, 1995). It should be emphasized that the stiffness constraint with the homogenized elasticity modulus cannot fully guarantee connectivity, however it performs well in practice for the problems considered here.

The optimization problems are solved using the Method of Moving Asymptotes (MMA) (Svanberg, 1987). In particular, the bound formulation stated in Eq. (29) can be solved by manipulating with the constants in MMA. This is a gradient-based algorithm that uses information from previous iteration steps and the computed sensitivities of the objective function. Thus the derivatives of the objective function and the constraint function with respect to the design variables must be evaluated.

3.2 Design sensitivity analysis

To update the design variables in the gradient-based topology optimization procedure, the derivative of the objective function with respect to the design variables, called design sensitivities, is computed. The sensitivity of η with respect to a single design variable γ_i is found as

$$\frac{\mathrm{d}\eta}{\mathrm{d}\gamma_i} = \frac{2}{(k')^2}\left(k'\left(\frac{\mathrm{d}k}{\mathrm{d}\gamma_i}\right)'' - k''\left(\frac{\mathrm{d}k}{\mathrm{d}\gamma_i}\right)' \right) \tag{31}$$

where $\mathrm{d}k/\mathrm{d}\gamma_i$ is found by taking the derivative of the discretized equation system in Eq. (24) with

respect to the design variable

$$\frac{\mathrm{d}}{\mathrm{d}\gamma_i}\left(\left(k^2\mathbf{M}-k\mathbf{C}+\mathbf{K}\right)\mathbf{U}\right)=\frac{\mathrm{d}k^2}{\mathrm{d}\gamma_i}\mathbf{M}\mathbf{U}+k^2\frac{\mathrm{d}\mathbf{M}}{\mathrm{d}\gamma_i}\mathbf{U}+k^2\mathbf{M}\frac{\mathrm{d}\mathbf{U}}{\mathrm{d}\gamma_i} -\frac{\mathrm{d}k}{\mathrm{d}\gamma_i}\mathbf{C}\mathbf{U}-k\frac{\mathrm{d}\mathbf{C}}{\mathrm{d}\gamma_i}\mathbf{U}-k\mathbf{C}\frac{\mathrm{d}\mathbf{U}}{\mathrm{d}\gamma_i}+\frac{\mathrm{d}\mathbf{K}}{\mathrm{d}\gamma_i}\mathbf{U}+\mathbf{K}\frac{\mathrm{d}\mathbf{U}}{\mathrm{d}\gamma_i}=0 \tag{32}$$

Collecting terms with $\mathrm{d}k/\mathrm{d}\gamma_i$ and rearranging yields

$$\frac{\mathrm{d}k}{\mathrm{d}\gamma_i}\left(2k\mathbf{M}-\mathbf{C}\right)\mathbf{U}+k^2\frac{\mathrm{d}\mathbf{M}}{\mathrm{d}\gamma_i}\mathbf{U}-k\frac{\mathrm{d}\mathbf{C}}{\mathrm{d}\gamma_i}\mathbf{U}+\frac{\mathrm{d}\mathbf{K}}{\mathrm{d}\gamma_i}\mathbf{U}+\left(k^2\mathbf{M}-k\mathbf{C}+\mathbf{K}\right)\frac{\mathrm{d}\mathbf{U}}{\mathrm{d}\gamma_i}=0 \tag{33}$$

In order to eliminate the unknown expression involving $\mathrm{d}\mathbf{U}/\mathrm{d}\gamma_i$ we define an adjoint variable problem. Eq. (33) is multiplied by adjoint vector $\mathbf{V}^{\mathrm{T}}$

$$\frac{\mathrm{d}k}{\mathrm{d}\gamma_i}\mathbf{V}^{\mathrm{T}}\left(2k\mathbf{M}-\mathbf{C}\right)\mathbf{U}+k^2\mathbf{V}^{\mathrm{T}}\frac{\mathrm{d}\mathbf{M}}{\mathrm{d}\gamma_i}\mathbf{U}-k\mathbf{V}^{\mathrm{T}}\frac{\mathrm{d}\mathbf{C}}{\mathrm{d}\gamma_i}\mathbf{U}+\mathbf{V}^{\mathrm{T}}\frac{\mathrm{d}\mathbf{K}}{\mathrm{d}\gamma_i}\mathbf{U}+\mathbf{V}^{\mathrm{T}}\left(k^2\mathbf{M}-k\mathbf{C}+\mathbf{K}\right)\frac{\mathrm{d}\mathbf{U}}{\mathrm{d}\gamma_i}=0 \tag{34}$$

We choose $\mathbf{V}^{\mathrm{T}}$ to solve the left eigenvalue problem defined as

$$\mathbf{V}^{\mathrm{T}}\left(k^2\mathbf{M}-k\mathbf{C}+\mathbf{K}\right)=0\Leftrightarrow\left(k^2\mathbf{M}-k\mathbf{C}+\mathbf{K}\right)^{\mathrm{T}}\mathbf{V}=0 \tag{35}$$

so that the last term in Eq. (34) vanishes and the remaining terms are

$$\frac{\mathrm{d}k}{\mathrm{d}\gamma_i}\mathbf{V}^{\mathrm{T}}\left(2k\mathbf{M}-\mathbf{C}\right)\mathbf{U}+k^2\mathbf{V}^{\mathrm{T}}\frac{\mathrm{d}\mathbf{M}}{\mathrm{d}\gamma_i}\mathbf{U}-k\mathbf{V}^{\mathrm{T}}\frac{\mathrm{d}\mathbf{C}}{\mathrm{d}\gamma_i}\mathbf{U}+\mathbf{V}^{\mathrm{T}}\frac{\mathrm{d}\mathbf{K}}{\mathrm{d}\gamma_i}\mathbf{U}=0 \tag{36}$$

Thus,

$$\frac{\mathrm{d}k}{\mathrm{d}\gamma_i}=\frac{\mathbf{V}^{\mathrm{T}}\left(k^2\frac{\mathrm{d}\mathbf{M}}{\mathrm{d}\gamma_i}-k\frac{\mathrm{d}\mathbf{C}}{\mathrm{d}\gamma_i}+\frac{\mathrm{d}\mathbf{K}}{\mathrm{d}\gamma_i}\right)\mathbf{U}}{\mathbf{V}^{\mathrm{T}}\left(\mathbf{C}-2k\mathbf{M}\right)\mathbf{U}} \tag{37}$$

where $\mathbf{V}$ is the left eigenvector of the discretized equation system in Eq. (24).

A further advantage of the adjoint method is that it can be readily implemented in commercial finite element software programs such as COMSOL. The reader is referred to the literature for more details and example code in a high-level programming language (Olesen et al., 2006).

4. Design example

An example is presented in order to demonstrate the effectiveness of the proposed design method and discuss the effect of the presence of the acoustic medium. The model problem is illustrated in Fig. 1(a). The aim is to distribute solid material and air in the designated design domain Ω_d surrounded by a fixed solid frame structure. The design domain is restricted to the interior part of the unit cell which allows us to impose periodic boundary conditions for the displacement components only. In order to enforce the required 45 degree symmetry, the computed sensitivities are averaged and numerically identical sensitivities are assigned in the symmetrical sections. The direction for the wave vector θ includes the three angles 0^o, 22.5^o, and 45^o and the frequencies of interest are $\omega_i \in [9\text{kHz}, 10\text{kHz}, 11\text{kHz}]$ which corresponds to a relatively low frequency range for the specific choice of unit cell dimensions. The constant filter radius R = 1 mm is used – corresponding to 0.1×L. For the stiffness constraint we set f_E = 0.25, so that the computed effective Young's modulus should be no less than 500 Mpa.

It was found that when we optimize the attenuation factor for higher frequencies, either for a frequency range or a single frequency, the optimized microstructure usually exhibits large bandgaps, i.e., frequency ranges in which waves cannot propagate. Even though we do not explicitly consider bandgaps in the optimization formulation, bandgap structures are automatically generated since they provide strong wave attenuation regardless of the presence of air. In this work we will concentrate on the more challenging lower frequency range where bandgaps are more difficult to create and the interaction to the lossy air medium can be utilized.

4.1 Results

Snapshots of the topology optimization process by different initial designs are shown in Fig. 3. The final design in Fig. 3(c) is the one that is ultimately used as our blueprint structure, whereas the additional optimization runs shown in Fig. 3(a) and (b) are included in order to show the effect of the initial design and have been terminated before final convergence. It is clear from the figure that the qualitative nature of the optimized designs is similar in the form of structural resonators inside confined air cavities, however, the detailed appearance of the designs differs.

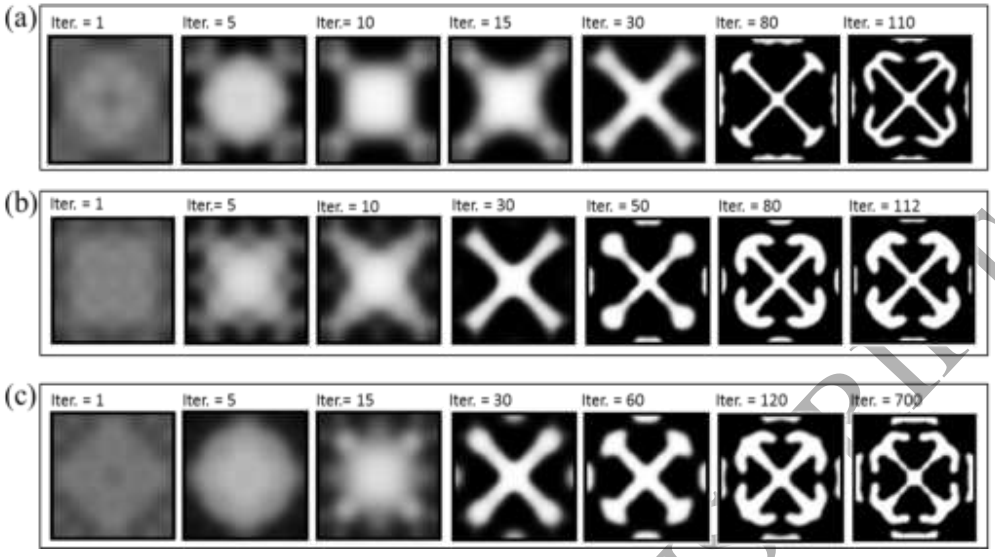

Figure 3 Snapshots of the topology optimization, starting with the randomly distributed material (initial design). (a) and (b) show additional optimization runs terminated before final convergence and (c) shows the converged result used for the final structure.

The final chosen microstructure optimized for the loss is presented in Fig 4 with Fig. 4(a) showing the optimized material distribution. The raw optimized design shows a clear and well defined separation of material and air, but in order to ensure that the final design has a clear boundary where the coupling between the pressure and the displacement field is specified, we define a threshold value (0.5) to eliminate any leftover gray scale elements in the final optimized design. From the resulting isosurfaces, a post-processed version of the design is the transferred to a CAD model. The resulting design is presented in Fig. 4(b) with a 3×3 unit cell illustration of the optimized material shown in Fig. 4(c).

The post-processed design is re-analyzed by using a segregated ASI model with 42804 triangular elements. When we compare the performance of this model to the raw optimized design analyzed with the mixed-FEM model, we note a frequency shift upward but do not see a significant deterioration in the general performance. In the following all results for the optimized design are based on the post-processed model and for comparison we also compute the performance for the pure structural problem with void replacing the acoustic cavities as well as for the coupled problem without dissipation in the acoustic media (only for loss computations).

The ASI problem and the pure structural problem with $\omega(\mathbf{k})$-formulation are solved for 20 points along the bounded line O-A-B-O. Additionally, the eigenvalue problem with $\mathbf{k}(\omega)$-formulation of the optimized design is solved to compute the loss factor in the frequency range $\omega \in [0,30]$ kHz. The real part of the band diagrams and the frequency response of loss factor are displayed in Fig. 5(a) and 5(b), respectively.

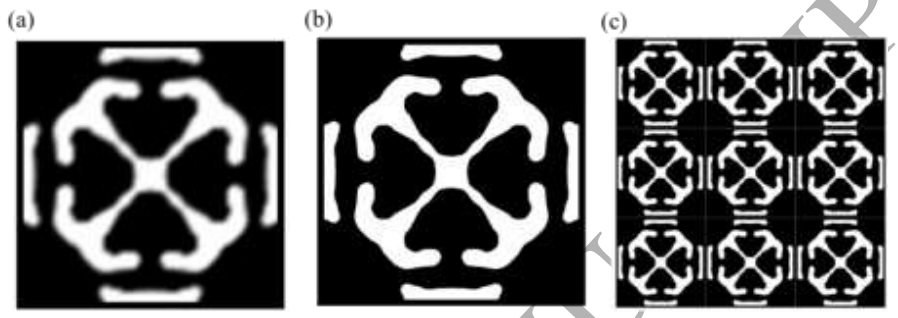

Figure 4 (a) Optimized elastic-acoustic microstructure. (b) Post-processed design with the threshold value 0.5. (c) 3x3 unit cells of the post-processed design.

When comparing the band diagrams for the ASI model (markers) and the void model (lines) in Fig. 5(a) an overall similar response is observed in general, which is expected seen in light of the numerical test conducted earlier. However, when looking at the enlarged figure in Fig. 5(c) displaying the frequency range from 9-12 kHz, some differences are observed with the ASI model exhibiting a frequency shift and most importantly additional acoustic modes which will be discussed and analyzed later.

The frequency bands for the optimized design in the vicinity of the optimization frequencies are characterized by significant distortion and flatness. As seen in Fig. 5(b) this is accompanied by an enhanced attenuation factor. Especially, we note the increase in the loss factor near the flat frequency bands in the 11-12 kHz interval. These flat frequency bands indicate that the increase in loss factor is caused by locally resonating structures in the unit cell. The resonating structures (acting as local tuned mass dampers) cause a high reflection of the waves and hence in Fig. 5(b) we can see that the loss (or attenuation) factor is fairly high for all of the models considered since the phenomenon inherently do not rely on the coupling to the acoustic medium nor the presence

of dissipation. However, it is clear from Fig. 5(b) that the predicted loss factor does show a significant increase when considering the fully coupled model with a lossy air medium. A similar observation was made in author's previous study for the enhancement of the damping ratio of a structure with embedded microbeam resonators in air-filled internal cavities (Kook and Jensen, 2014).

We have solved the corresponding eigenvalue problem in order to investigate the locally resonating structures in the unit cell. The selected modes are presented in Fig. 6 when $k_y = 0$ and $k_x = \pi / L$. As we expect, the local character of the modes is clearly noted. We also see similar mode shapes in other flat and distorted bands. In order to further investigate the presence of the acoustic resonances noted as the flat bands around 10.2 khz, we conduct an eigenvalue analysis for the large acoustic cavity in the unit cell. The resulting acoustic modes are presented in Fig. 7. It reveals that the first 3 acoustic modes match the flat frequency bands. The eigenfrequencies are 10329Hz, 10329Hz, and 10516 Hz where the multiple solutions are due to the symmetry of the cavity. These frequency bands are indicated in Fig. 5(c).

This example clearly shows that the combination of a locally resonating micro structure in the unit cell with a resonance frequency in the close vicinity of an acoustic resonance, may lead to a significant increase in the loss. With the aid of the developed topology optimization method we have shown that it is possible to design the unit cell so that this favorable combination of frequencies appears.

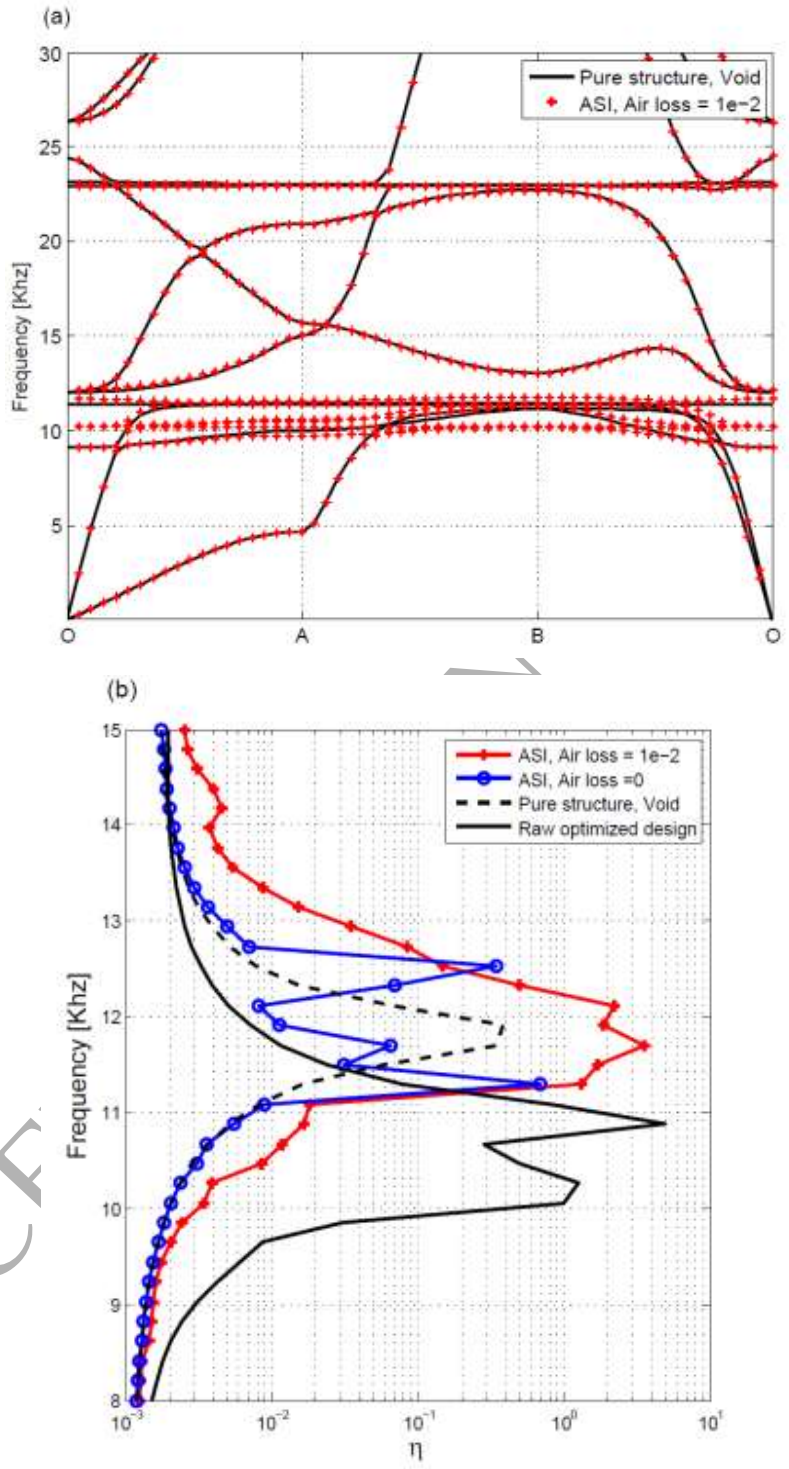

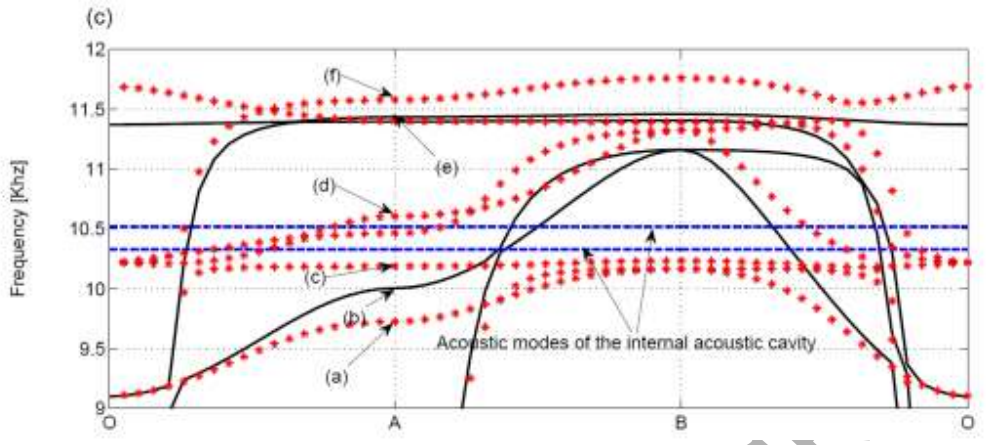

Figure 5 (a) Band diagram for the optimized microstructure in Fig. 4. (b) Performance of the optimized design in terms of loss factor as function of frequency. (c) Enlarged figure in the frequency from 9-12 kHz

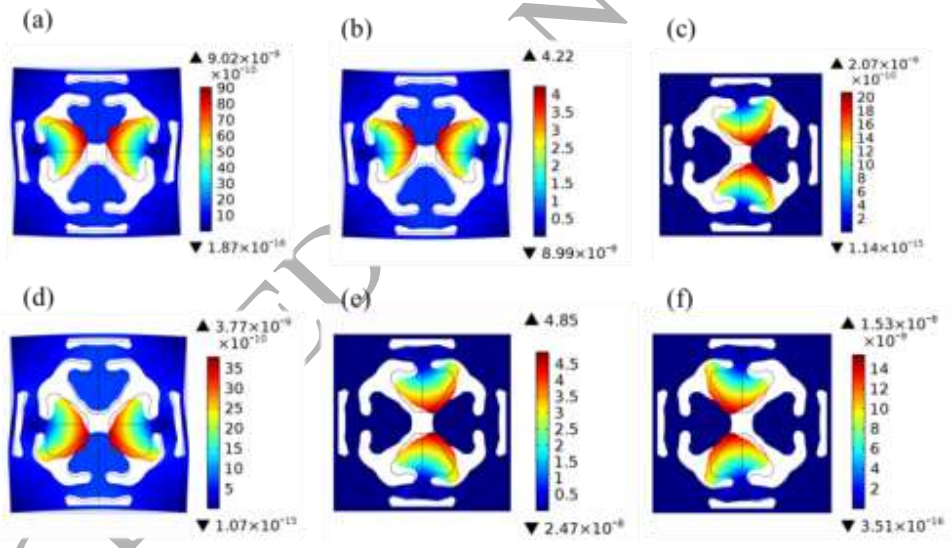

Figure 6 Mode shape at the indicating frequencies in Fig. 5(c), Total displacement [m].

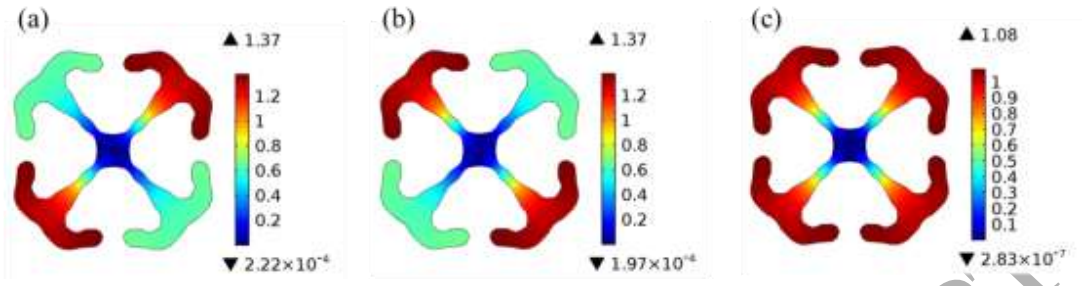

Figure 7 Acoustic modes of the internal acoustic cavity in the optimized unit cell. (a) and (b) are the first and second modes with 10329 Hz, and (c) the third modes with 10516 Hz.

It should be noted that the choice of air loss factor in the phenomenological model is important for the optimization procedure. Our experience shows that using a value of 0.01 or *smaller* results in qualitatively similar designs, where the enhanced total loss factor is created by the resonating structures. However, increasing the value of the air loss factor to 0.1 or higher results in poor designs that are difficult to interpret including disconnected solid parts and many acoustic cavities. We speculate that this is due to the fact that the intrinsic air loss now dominates which makes resonating structures less favorable and promotes a seemingly arbitrary appearance of air cavities.

The phenomenological model to include acoustic losses is a simplification and does not take into account the physical origin of the acoustic losses from the viscous and thermal boundary layers. These are of fundamental importance with small geometrical features, however, including a proper thermo-viscous acoustic model in the optimization procedure is beyond the scope of this paper. Instead, we evaluate the performance of the optimized design with the thermo-viscous acoustical model.

The performance evaluation is performed by calculating the modal damping ratio (MDR) from an eigenvalue analysis of the optimized unit cell. To simplify the analysis the Bloch-wave condition has been omitted, thus we consider the unit cell as a free structure. We use the thermoacoustic-structure interaction model in COMSOL Multiphysics using standard properties for air (with zero bulk viscosity). We employ a very fine mesh near isothermal boundaries, i.e. boundaries between the structure and the acoustic domain, to be able to accurately resolve the

viscous and thermal boundary layers. For comparison purposes, we also calculated the modal properties for the design with void instead of acoustic cavities. Here, the computed MDRs is governed by the structural loss factor as $\eta_{sol}/2 = 5.000e-04$.

Table 1. The eigenfrequencies and MDRs for the unit cell structure. An eigenvalue analysis yields a set of complex values, $\lambda_i = \pm\sqrt{\beta_i} = \omega_i + i\alpha_i$ where $\mathrm{Re}(\lambda_i) = \omega_i$ and $\mathrm{Im}(\lambda_i) = \alpha_i$. MDR corresponding to the i^{th} eigenfrequency is obtained by $\varsigma_i = \alpha_i \Big/ \sqrt{\alpha_i^2 + \omega_i^2}$.

Eigen Solution	Void (No Air)	ASI (phenomenological model, $\eta_{air} = 0.01$)	ASI (Thermoacoustic model)
ω_1	3614.3	3606.6	3605.8
α_1	1.8071	1.8205	3.2933
ς_1	5.0000e-4	5.0477e-4	9.1333e-4
ω_2	8795.4	8798.2	8798.1
α_2	4.3977	4.3997	4.5474
ς_2	5.0000e-4	5.0007e-4	5.1686e-4
ω_3	8936.8	8841.2	8823.8
α_3	4.4684	9.0397	41.664
ς_3	5.000e-4	0.0010225	0.0047217
ω_4	8936.8	8841.2	8823.8
α_4	4.4684	9.0397	41.661
ς_4	5.0000e-4	0.0010225	0.0047214
ω_5	9423.1	9423.6	9423.7
α_5	4.7115	4.7123	4.7383
ς_5	5.0000e-4	5.0005e-4	5.0281e-4
ω_6	16994	10445	10113
α_6	8.4968	98.839	343.09
ς_6	4.9997e-4	0.0094626	0.033018

The results are summarized in Table 1 and the mode shapes for the first 5 modes are shown in Fig. 8. It is clear that the qualitative nature of the modes shapes resemble the modes found for the full wave analysis and displayed in Fig. 6. From the table it is seen that the phenomenological model captures the modal frequencies reasonably well, but underestimates MDR. However, the significant increase in MDR found for the modes near 9 kHz is seen for

both models. Also, the high MDR computed for the 6th mode (pure acoustic mode for the ASI models) supports the qualitative agreement between the results.

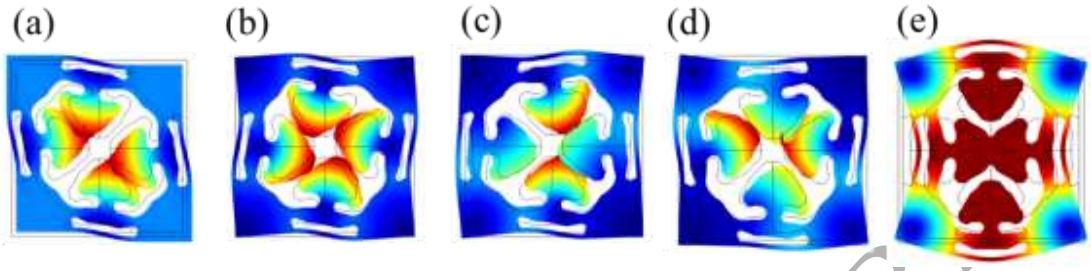

Figure 8. First 5 mode shapes of the optimized unit cell structure modelled with a full thermoacoustic-structure interaction model.

5. Conclusion

In this paper we have presented a gradient-based topology optimization method for the design of 2D periodic structures with a lossy acoustic medium for maximizing the loss/attenuation of propagating waves. The work encompassed the derivation of a computational model based on a mixed displacement and pressure finite element discretization of a periodic unit cell and a complex eigenvalue problem with a prescribed frequency. Maximization of the loss in a target frequency range was considered as the objective function for the optimization in order to obtain the largest possible wave attenuation by combining the effects of favorable distribution of solid material and an acoustic medium with dissipation. In the design example we found that the optimized design has a locally resonating internal structure combined with acoustic modes with frequencies close to those of the resonators. It was shown that the acoustic-structure interaction in the optimized microstructure caused an increased overall loss factor and that the presence of the lossy acoustic medium had strong effect on the wave decay of the periodic structure. We conclude that the proposed loss optimization presented here works well for creating a favorable distribution of a lossy acoustic medium and a stiff constituent in order to enhance the damping properties of the composite material.

Acknowledgements

The work of J.K. was funded by the Danish Research Agency through the innovation consortium FMAT and by the Danish Council for Independent Research - Individual postdoctoral grants.

References

Andreasen, C.S., Andreassen, E., Jensen, J.S., Sigmund, O., 2014. On the realization of the bulk modulus bounds for two-phase viscoelastic composites. Journal of the Mechanics and Physics of Solids 63, 228-241.

Andreassen, E., Jensen, J.S., 2013a. Analysis of phononic bandgap structures with dissipation. Journal of Vibration and Acoustics 135.

Andreassen, E., Jensen, J.S., 2013b. Topology optimization of periodic microstructures for enhanced dynamic properties of viscoelastic composite materials. Structural and Multidisciplinary Optimization 49, 695-705.

Andreassen, E., Lazarov, B.S., Sigmund, O., 2014. Design of manufacturable 3D extremal elastic microstructure. Mechanics of Materials 69, 1-10.

Bloch, F., 1929. Über die Quantenmechanik der Elektronen in Kristallgittern. Zeitschrift für Physik 52, 555-600.

Halkjær, S., Sigmund, O., Jensen, J.S., 2006. Maximizing band gaps in plate structures. Structural and Multidisciplinary Optimization 32, 263-275.

Kook, J., Jensen, J.S., 2014. Analysis of enhanced modal damping ratio in porous materials using an acoustic-structure interaction model. A I P Advances 4.

Cremer, L., Heckl, M., Petersson, Björn A.T., 2005. Structure-Borne Sound; Structural Vibrations and Sound Radiation at Audio Frequencies. Springer-Verlag Berlin Heidelberg.

Bendsoe, M.P., Sigmund, O., 2004. Topology Optimization, Theory, Methods, and Applications. Springer-Verlag Berlin Heidelberg.

Meaud, J., Sain, T., Hulbert, G.M., Waas, A.M., 2013. Analysis and optimal design of layered composites with high stiffness and high damping. International Journal of Solids and Structures 50, 1342-1353.

Moiseyenko, R.P., Laude, V., 2011. Material loss influence on the complex band structure and group velocity in phononic crystals. Physical Review B 83, 064301.

Olesen, L.H., Okkels, F., Bruus, H., 2006. A high-level programming-language implementation of topology optimization applied to steady-state Navier–Stokes flow. International Journal for Numerical Methods in Engineering 65, 975-1001.

Bilal, O.R., Hussein, M.I., 2011. Ultrawide phononic band gap for combined in-plane and out-of-plane waves. Physical Review E 84, 065701.

Pedersen, N.L., 2014. Maximization of eigenvalues using topology optimization. Structural and Multidisciplinary Optimization 20, 2-11.

Picelli, R., Vicente, W.M., Pavanello, R., Xie, Y.M., 2015. Evolutionary topology optimization for natural frequency maximization problems considering acoustic–structure interaction. Finite Elements in Analysis and Design 106, 56-64.

Shu, L., Yu Wang, M., Ma, Z., 2014. Level set based topology optimization of vibrating structures for coupled acoustic–structural dynamics. Computers & Structures 132, 34-42.

Sigmund, O., 1995. Tailoring materials with prescribed elastic properties. Mechanics of Materials 20, 351-368.

Sigmund, O., Clausen, P.M., 2007. Topology optimization using a mixed formulation: An alternative way to solve pressure load problems. Computer Methods in Applied Mechanics and Engineering 196, 1874-1889.

Sigmund, O; Maute, K., 2013. Topology Optimization Approaches - A Comparative Review. Structural and Multidisciplinary Optimization 48, 1031-1055

Sigmund, O., Torquato, S., 1997. Design of materials with extreme thermal expansion using a three-phase topology optimization method. Journal of the Mechanics and Physics of Solids 45, 1037-1067.

Svanberg, K., 1987. The method of moving asymptotes—a new method for structural optimization. International Journal for Numerical Methods in Engineering 24, 359-373.

Søndergaard, M.B., Pedersen, C.B.W., 2014. Applied topology optimization of vibro-acoustic hearing instrument models. Journal of Sound and Vibration 333, 683-692.

Vicente, W.M., Picelli, R., Pavanello, R., Xie, Y.M., 2015. Topology optimization of frequency responses of fluid–structure interaction systems. Finite Elements in Analysis and Design 98, 1-13.

Wang, F., Lazarov, B.S., Sigmund, O., 2010. On projection methods, convergence and robust formulations in topology optimization. Structural and Multidisciplinary Optimization 43, 767-784.

Wang, X., Bathe, K.-J., 1997. Displacement/pressure based mixed finite element formulations for acoustic fluid–structure interaction problems. International Journal for Numerical Methods in Engineering 40, 2001-2017.

Wang Y-F, Wang Y-S, Laude V., 2015, Wave propagation in two-dimensional viscoelastic metamaterials. Physical Review B 92, 104110

Yoon, G.H., Jensen, J.S., Sigmund, O., 2007. Topology optimization of acoustic–structure interaction problems using a mixed finite element formulation. International Journal for Numerical Methods in Engineering 70, 1049-1075.